Chapter 1

Kinematic ray tracing in anisotropic layered media

The first step toward estimating tomographically elliptical velocities in heterogeneous anisotropic media is to be able to do ray tracing. In this chapter, I review a procedure to trace rays in layered transversely isotropic models with dipping interfaces. Group velocities are used to propagate the ray across each homogeneous layer, and phase velocities are used to find out how a given ray changes its direction when impinging on an interface. The equation that relates the ray parameter of the incident ray with the angle of the emergent phase at each interface is studied in detail. Finally, examples of ray tracing in simple anisotropic models are shown.

1.1 Introduction

Estimating velocity anisotropy tomographically from cross-well traveltime data is a process that often has two kinds of nonlinearity: the anisotropy itself and the ray bending from one iteration to the next. Under certain conditions one of these nonlinearities can be neglected while the computations related to other one are simplified. For example, assuming weak anisotropy, Pratt and Chapman (1992), and Chapman and Pratt (1992) proposed to do the ray tracing in isotropic media and to use those rays to back project in the anisotropic model. As I show in chapter 4, the problem can be simplified even more if the velocity contrasts are small enough that the rays traced on the anisotropic model are straight and the only nonlinearity that remains is in the estimation of the anisotropy. Unfortunately, these simplifications are not generally valid and therefore the problem needs to be solved by tracing rays appropriately in inhomogeneous anisotropic media.

Methods for dynamic ray tracing in inhomogeneous anisotropic media have been proposed by Červený (1972), Hanyga (1982), Jech and Pšenčík (1989), and Gajewski and Pšenčík (1990), among others. These methods are based on the solution of the dynamic ray tracing equations. To solve only the kinematic problem (what is needed to do traveltime tomography), Byun (1982, 1984) proposed a different technique based on the application of Snell's law at each interface.

In this chapter, I review and implement Byun's procedure for kinematic, anisotropic ray tracing. From the boundary conditions at each interface, I derive the equation that relates the ray parameter p of the incident phase to the angle of the transmitted phase. Using this equation and the equations that relate phase and group velocities, I describe a procedure that alternatively uses each type of velocity to propagate a ray across a layer and to figure out how it changes direction when impinging on an interface. The last section gives examples of P-wave ray tracing for a cross-well geometry in different layered transversely isotropic models. In chapter 4, I use this ray tracing procedure to do traveltime tomography in elliptically azimuthally anisotropic media.

1.2 Boundary conditions

A wave impinging on a plane interface between two media must satisfy the kinematic boundary condition

$$\mathbf{v}_1 \;=\; \mathbf{v}_1, \tag{1.1}$$

which states that the particle velocity must be continuous at all points on the boundary between medium 1 and medium 2 (Auld, 1990).

If the wave field is described as a superposition of functions of the form $\exp(\imath\mathbf{kr})$, the condition (1.1) implies that for both incident and scattered waves the component of $\mathbf{k}$ tangential to the boundary ($\mathbf{k}_{||}$) must be the same. If we divide $\mathbf{k}$ by the frequency ω of the incident wave and define a vector $\tilde{\mathbf{k}}$ of magnitude $1/v$ (where v is the phase velocity) as follows:

$$\tilde{\mathbf{k}} \;=\; \frac{\mathbf{k}}{\omega} \;=\; \frac{\mathbf{k}}{||\mathbf{k}||}\frac{1}{v}, \tag{1.2}$$

the continuity of $\mathbf{k}_{||}$ implies the continuity of $\tilde{\mathbf{k}}_{||}$, usually called ray parameter $\mathbf{p}$ for which

$$\mathbf{p_1} \;=\; \mathbf{p_2}. \tag{1.3}$$

Since we know that $\mathbf{p}$ is parallel to the interface, the ray parameter is usually considered as a scalar p with a positive or negative sign in front to indicate the sign of the angle of the incident phase with respect to the normal.

Auld (1990) examines condition (1.3) by looking at the corresponding slowness surfaces (a plot of $||\tilde{\mathbf{k}}||$ as a function of its direction), as Figure 1.1 shows. In this figure the slowness surfaces for both P- and S-waves are represented for each isotropic medium. The vector $CA = AB = \mathbf{p}$ is the projection on the interface of the point on the slowness surface that corresponds to the incident P-wave phase. From the construction of Figure 1.1 it is possible to derive easily Snell's law that gives the angles of the scattered phases for both P- and S-waves:

$$p \;=\; \frac{1}{v_{1_P}}\sin(\theta_{P_i}) \;=\; \frac{1}{v_{2_P}}\sin(\theta_{P_t}) \;=\; \frac{1}{v_{2_S}}\sin(\theta_{S_t})$$

$$= \frac{1}{v_{1_S}} \sin(\theta_{S_r}) = \frac{1}{v_{1_P}} \sin(\theta_{P_r}). \tag{1.4}$$

Figure 1.1: Plane-wave scattering at a plane boundary between two isotropic media. From this construction Snell's law can be easily derived. Ray and phase directions are equal. slow-surf [NR]

Snell's law tells us how a given phase changes its direction when it crosses the interface between two media. It also tells us how rays change direction when crossing an interface, but the medium must be isotropic for this to be true, as in Figure 1.1. In isotropic media, since rays and waves travel in the same direction with the same velocity, boundary conditions valid for waves are also used to predict the behavior of rays. In anisotropic media, however, this simplification is no longer valid because, in general, rays and waves travel with different velocities in different directions as shown in Figure 1.2.

1.3 Initial value ray tracing

When the medium is horizontally layered and isotropic, tracing a ray across the different interfaces is easy. From the medium's velocities and the direction of the ray at the source (p), successive applications of (1.4) tell us how a ray changes its direction as it travels. The only angles that matter are those of the incident and refracted rays. If the layers dip the problem is slightly more complicated because p has to be calculated every time the ray reaches a new interface and we have to consider with three instead of two angles at each boundary.

When the medium is anisotropic, we have to consider with seven angles at each interface to figure out how a ray changes its direction. All these angles (positive

Figure 1.2: Plane-wave scattering at a plane boundary between two anisotropic media. The slowness surfaces are separated and nonspherical. Ray directions (dashed arrows at the slowness surfaces) and phase directions (continuous arrows) are no longer the same.(Modified from Aki and Richards, 1980.) slow-surf-ani [NR]

counterclockwise) are shown in Figure 1.3. The continuity of the slowness across the interface [equation (1.3)] is expressed as follows:

$$p = \frac{\sin(\theta_i + \gamma_1)}{v_1(\theta_i)} = \frac{\sin(\theta_t + \gamma_2)}{v_2(\theta_t)}, \tag{1.5}$$

where $v_1(\theta_i)$ and $v_2(\theta_t)$ are the phase velocities in the corresponding media evaluated at the incident and transmitted phase angles, respectively. The sums $(\theta_i + \gamma_1)$ and $(\theta_t + \gamma_2)$ have to be calculated considering the proper signs of the angles. From equation (1.5) we can see that when $p = 0$ (normal incidence) the angle of the transmitted phase does not depend on the phase velocity and is $\theta_t = -\gamma_2$. Any other relation derived from (1.5) must reproduce this simple result.

Given the function $v(\theta)$ for each medium, equation (1.5) describes how the incident phase $\tilde{\mathbf{k}}$ changes its direction when crossing the interface between two media. However, (1.5) does not show what happens to the direction and velocity of the associated ray. These two quantities can be calculated from the equations that relate phase and ray velocities (Byun, 1984):

$$v(\theta) = V(\phi)\cos(\phi - \theta), \tag{1.6a}$$

$$\tan(\phi - \theta) = \frac{1}{v(\theta)}\frac{dv(\theta)}{d\theta}, \tag{1.6b}$$

$$V^2(\phi) = v^2(\theta) + \left(\frac{dv(\theta)}{d\theta}\right)^2, \tag{1.6c}$$

where $V(\phi)$ is the ray velocity along the ray angle ϕ.

Figure 1.3: Incident (i) and transmitted (t) group and phase angles of a ray impinging on a plane interface between two transversely isotropic media. all-angles [NR]

Equations (1.5) and (3.6) are the basic relations for tracing a ray in a medium where $v(\theta)$ and γ are given for each layer. Byun (1984) proposes the following procedure to do so: (1) Assign a value to $\theta = \theta_i$ at the source position. (2) Repeat the next steps for each layer: (a) Evaluate $v(\theta)$ and $\frac{dv(\theta)}{d\theta}$ at the corresponding θ. (b) Find ϕ_t and $V(\phi_t)$ from equation (3.6). (c) Trace a ray along the angle ϕ_t until it reaches the next interface. (d) Find p of the incident wave using equation (1.5). (e) Solve equation (1.5) for θ_t. (3) Return to step 2a.

The previous ray tracing procedure is valid for any phase velocity function $v(\theta)$. What changes from one choice of the velocity function to another is how to solve step 2e [to find θ_t as a function of p using equation (1.5)]. The next section focuses on how to accomplish this step when the medium is transversely isotropic.

1.4 Solving for the phase angle

1.4.1 P- and SV-waves

In a transversely isotropic medium, the phase velocity $v(\theta)$ for P- and SV-waves is expressed as follows (Auld, 1990):

$$
\begin{aligned}
2\rho v^2(\theta) &= c_{11}\sin^2(\theta) + c_{33}\cos^2(\theta) + c_{44} \qquad (1.7)\\
&\pm \sqrt{[(c_{11}-c_{44})\sin^2(\theta) + (c_{44}-c_{33})\cos^2(\theta)]^2 + (c_{13}+c_{44})^2\sin^2(2\theta)},
\end{aligned}
$$

where c_{ij} are four of the five elastic constants that describe a homogeneous transversely isotropic medium. The plus sign $(+)$ in front of the square root corresponds to P-waves and the minus sign $(-)$ to SV-waves. ρ is the density.

An equation for the transmitted phase angle θ_t as a function of the incident p can be obtained by substituting equation (1.7) into equation (1.5) which results in the following fourth-order polynomial in $\tan(\theta_t)$:

$$a_0 + a_1 \tan(\theta_t) + a_2 \tan^2(\theta_t) + a_3 \tan^3(\theta_t) + a_4 \tan^4(\theta_t) \;=\; 0, \qquad (1.8)$$

where the coefficients a_i are given in appendix ??. A similar expression obtained by Byun (1984) is not correct because $\theta_t = -\gamma_2$ is not a root of the polynomial when $p = 0$, as equation (1.5) predicts.

As shown in appendix ??, the coefficients a_i are the same for both P- and SV-waves [the ± in front of the square root in equation (1.7) is lost in the derivation of (1.8)], and they are independent of the sign of p. In principle, by solving this equation at each interface, it should be possible to find the angle of the transmitted phase by computing the arctangent of one of its roots. However, the procedure is not straightforward. On the one hand, we have to identify the solutions that correspond to p or $-p$ and P- or SV-waves. On the other hand, finding an angle from its tangent is not a one-to-one transformation because $\tan(\theta) = \tan(\theta + n\pi)$ and therefore infinite angles satisfy equation (1.8). Aside from these problems, we usually have to deal with the difficulties of solving equation (1.8) numerically.

Let's first examine the numerical problems. It is well known that most algorithms used to find roots of polynomials fail in the presence of multiple (or close to multiple) roots. This is the case with equation (1.8) when $p = 0$. From equation (1.5), we find that in this case the transmitted phase angle is $\theta_t = -\gamma_2$ and therefore it is not necessary to solve equation (1.8) when $p = 0$. Problems may also arise when $p \approx 0$ because the roots are close to being multiple. The way I found around this problem is based on the assumption that the slowness surface is a smooth function of θ and that therefore when $p \approx 0$, $v_2(\theta_t) \approx v_2(-\gamma)$. If this is true, $\theta_{t_0} = -\gamma_2$ can be used as starting point to find θ_t by successive applications of equation (1.5) as follows:

$$\theta_{t_{i+1}} \;=\; \sin^{-1}(p v_2(\theta_{t_i})) - \gamma_2. \qquad (1.9)$$

Typically, only one iteration is required.

Figure 1.4 shows how to solve equation (1.8) graphically. From the construction with the slowness surfaces, we can see that the infinite roots of equation (1.8) mentioned earlier in this section correspond to only eight different points in the slowness surfaces for both P- and SV-waves. In this figure I also assume that the incident phase (not shown) is crossing the interface from medium 1 to medium 2. For simplicity, I assume that both media are isotropic. The slowness surfaces in medium 2 are represented half by continuous circles and half by dotted circles. The slowness surfaces in medium 1 are not shown. For a given $\pm p$ value at the interface, this figure shows the position of all the possible points in the P and SV slowness surfaces whose angle measured from the symmetry axis satisfies equation (1.8). These points are obtained by simple application of the kinematic boundary condition (1.3). The points A, B, C, and D are the solutions for negative p and the points H, G, F, and E, obtained by adding $\pm\pi$ to the previous solutions are the solutions for positive p. If $|p| > \frac{1}{v_p}$, two of the roots of (1.8) are complex and there are no transmitted P-waves. If $|p| > \frac{1}{v_s}$, the four roots are complex and there are no transmitted SV-waves either. I assume that when the transmitted ray travels parallel to the interface, it doesn't go back to the previous medium, which is a simplification of the actual behavior of head waves.

If we take "1" as the axis of symmetry in Figure 1.4, we see that when the axis of symmetry and the normal to the interface are parallel, the arctangent of the roots of equation (1.8) give the angles of the points A, B, E, and F. This is because the FORTRAN function ATAN gives its results in the interval $(-\pi/2, +\pi/2)$, which is exactly the domain of the phase angle measured from the axis of symmetry. "2" is also an axis of symmetry in this example because the medium is isotropic. If we take "2" as the axis of symmetry, the roots of equation (1.8) give the points E, F, G, and H. None of these points is the correct one when, for example, a P-wave impinges on the interface with negative p. In this case, the point B is the solution.

The preceding example tells us that when the axis of symmetry and the normal to the interface are not parallel, the roots of equation (1.8) may not give the expected direction for the refracted phase. For this reason, it is necessary to examine all eight angles and pick the one that verifies equation (1.5) for the desired wave type (with this, the number of possible angles is reduced from eight to two) and produces a ray pointing toward the expected direction (which further reduces the number of angles from two to one). This procedure will be explained in more detail in the next section, which concerns SH-waves.

Figure missing !

Figure 1.4: Graphical solution for the angle of the transmitted phase as a function of the incident p. The tangent of the angles at A, B, C, D, E, F, G, and H are roots of equation (3.8). Among these eight angles, only one reproduces the incident p for the corresponding wave type in the expected direction. When solving equation (3.8) numerically, only those angles at ±90 degrees from the axis of symmetry are obtained. The axes of symmetry 1 and 2 are two of the possible axes of symmetry of the isotropic medium in which the transmitted phase travels. $\boxed{\text{eight-roots}}$ [NR]

1.4.2 SH-waves

SH-waves in a transversely isotropic medium have elliptical slowness and wave surfaces. An elliptical slowness surface may not be a good *global* (i.e., for all angles) approximation for a P or SV slowness surface in a transversely isotropic medium, but it is a good *paraxial* approximation. Hence the importance of elliptical anisotropy in data fitting, specially when the measurements have limited aperture, as I explain in chapter 2.

The procedure explained in the preceding section for P- and SV-waves can be also used to trace rays when the medium is elliptically anisotropic. To see how this can be done, let's first rewrite the expression for the phase velocities (1.7):

$$\begin{aligned} 2\rho v^2(\theta) &= (c_{11}-c_{44})\sin^2(\theta)+(c_{33}-c_{44})\cos^2(\theta)+2c_{44} \\ &\pm \Big([(c_{11}-c_{44})\sin^2(\theta)+(c_{33}-c_{44})\cos^2(\theta)]^2 \\ &+ [(c_{13}+c_{44})^2-(c_{11}-c_{44})(c_{33}-c_{44})]\sin^2(2\theta)\Big)^{1/2}. \end{aligned}$$

To convert this equation into that of an ellipse (or a circle), we need to zero the coefficient of $\sin^2(2\theta)$ inside the square root. This is done by choosing

$$c_{13} = \sqrt{(c_{11}-c_{44})(c_{33}-c_{44})}-c_{44}.$$

This substitution, however, doesn't simplify the numerical computations.

Byun (1982) shows an alternative way to do the ray tracing that is computationally simpler than using the procedure for P- and SV-waves. He shows that when the slowness surfaces are elliptical the calculation at each interface of the refracted ray angle ϕ_t is simpler, because the phase angle θ_t does not need to be explicitly computed. Byun's expression for the ray parameter as a function of the ray's angle at each interface is

$$p = \frac{v_{\|}^{-2}\sin(\gamma_2)+v_{\perp}^{-2}\cos(\gamma_2)\tan(\phi_t)}{\sqrt{v_{\|}^{-2}+v_{\perp}^{-2}\tan^2(\gamma_2)}}, \tag{1.10}$$

where $v_{\|}$ and $v_{\perp}$ are the *SH*-wave velocities in the directions parallel and perpendicular to the axis of symmetry. After doing some algebra it is possible to solve for the ray angle ϕ_t, which yields

$$\tan(\phi_t) = \left(\frac{v_{\perp}}{v_{\|}}\right)\frac{sin(\gamma_2)\cos(\gamma_2)\pm\sqrt{v_{\|}^2\cos^2(\gamma_2)+v_{\perp}^2\sin^2(\gamma_2)-(pv_{\|}v_{\perp})^2}}{p^2v_{\perp}^2-\cos^2(\gamma)}. \tag{1.11}$$

Since equation (1.11) is independent of the sign of p, it gives the solutions of (1.10) for both positive and negative p. The correct ϕ_t is the one that gives the expected sign of p and corresponds to a ray in the desired direction.

If we take the extra step of solving explicitly for the phase angle at each interface, we have to choose among the four different points in the slowness surface whose angles satisfy equation (1.5), the one that produces a ray pointing in the desired direction.

The “desired direction” depends on the type of problem for which the ray tracer is used. Figure 1.5 shows how to pick the roots that correspond to transmitted rays, the ones needed in transmission traveltime tomography. In this figure, the horizontal distance from the center of the each ellipse to the vertical line is equal to the incident p. As we see, to obtain transmitted rays (dashed arrows with a black head), it is enough to pick the root that produces a ray pointing toward medium 2. In some cases the transmitted ray can travel parallel to the interface with the phase direction (continuous arrows) parallel to it or not (Figures 1.5f and 1.5e, respectively). The emergent phase angle may be greater than 90 degrees for the transmitted ray, as shown in Figure 1.5g. The ray pointing toward medium 2 may also go backwards, as Figure 1.5h shows. When the vertical line doesn't intersect the ellipse, there are no transmitted but only reflected rays (in which the angle of incidence is greater than the critical angle). However, to keep track more easily of the rays that hit the interface at post-critical angles, I assume that they continue traveling along the interface. The inversion procedure described in chapter 4 doesn't use these rays.

1.5 Model of heterogeneities

In this chapter, the rays are traced in heterogeneous models that are superposition of homogeneous transversely isotropic layers with dipping interfaces. The interfaces are not allowed to cross within the area of interest. Each layer is defined by the intersects and dips of the boundaries, the five elastic constants that define a transversely isotropic medium and the orientation of the axis of symmetry with respect to the vertical. When the anisotropy is elliptical, the five elastic constants are substituted by the velocities in the direction parallel and perpendicular to the axis of symmetry. This type of model simplifies the two-point ray tracing procedure described in the next section.

1.6 Two-point ray tracing

In transmission traveltime tomography, we usually need to link every source with the corresponding receiver positions. I do this, with the initial value ray tracing described in sections 3.3 and 3.4, as follows:

1. A sparse fan of rays is traced from the given source position. The aperture of this fan is greater than the aperture of the receiver positions. The end points of these rays (z_{end}) and the shooting angles (α_{init}) are saved.

2. The angle α_{init} that corresponds to a given receiver location is obtained (by using splines interpolation) from the relation α_{init} as a function of z_{end}. This relation is a function almost everywhere. In some places it can be multivalued because the same receiver location can correspond to different shooting angles (all of them greater than the critical angle). The points at which the function

Figure missing !

Figure 1.5: Roots of equation (3.5) (scattered phase angles) for negative p when the slowness surface is elliptical. Only the slowness surface in medium 2 is shown. In each case, the incident p is measured from the center of the ellipse to the vertical line. Continuous arrows show the scattered phase directions that correspond to transmitted rays (dashed arrows with a black head). Dashed arrows with a white head show ray directions with the same p but pointing towards medium 1. (a) Most common case. (b) Normal incidence ($p = 0$). (c) Phase direction parallel to the interface, ray not. (d) Two phase directions less than 90 degrees. (e) Ray direction parallel to the interface,

is multivalued must be removed before the interpolation. Because of the way the heterogeneities are described, α_{init} as a function of z_{end} always increases or always decreases (except where multivalued at post-critical angles or at triplications).

3. A ray is traced along the newly found α_{init}, and the z_{end} that results is compared to the expected receiver position. If the difference is greater than a predetermined value, I update the table α_{init} as a function of z_{end} is updated with the latest values of α_{init} and z_{end}, and return to step (2). If the difference is smaller than a predetermined value, the ray has been captured.

1.7 Examples

The following examples, show fans of P-wave ray paths in different models for a cross-well configuration. The fans are traced at constant intervals in the phase angle that only correspond to constant intervals in the ray angle when the medium is isotropic. This is shown in Figure 1.6a, where rays have been traced in the simplest model: homogeneous isotropic. When the model is transversely isotropic with vertical axis of symmetry, the density of rays changes with the angle, as Figure 1.6b shows. Figure 1.6c shows the ray paths in a homogeneous transversely isotropic model in which the axis of symmetry is tilted with respect to the vertical ($\gamma = 30$). When two-point ray tracing for the same receiver positions is performed in the corresponding homogeneous models, we don't see any difference among the three ray path diagrams because the ray angles depend only on the relative positions of source and receivers. The three cases differ only in the traveltimes.

Models like the ones shown in Figure 1.7 may arise from different combinations of deposition, erosion, and rotation of the layers involved. The finely layered areas can be modeled as homogeneous anisotropic layers with axis of symmetry perpendicular to the layering. The only difference between the two models in Figure 1.7 is in the axis of symmetry of the third layer. Figure 1.8 show the rays traced through these models for a source at 3500 feet. The elastic constants for each layer are listed in Table 1.1.

To check the accuracy of calculated P- and SV-wave traveltimes, I ran a finite-difference anisotropic elastic modeling algorithm (Karrenbach, 1992) using the layered model shown in Figure **??**, assuming a VSP geometry with the source at the surface separated 390 feet from the receiver well. The ray tracing was performed on the same model. Figure **??** shows the results of both the finite-difference elastic modeling and the anisotropic ray tracing. The first arrivals for P- and SV-waves predicted by the finite-difference modeling agree with the traveltimes computed by ray tracing. By picking the appropriate root in equation (1.8), reflections or conversions at the interfaces can also be modeled with ray tracing. Figure **??** also shows the traveltimes of reflected arrivals from a selected interface.

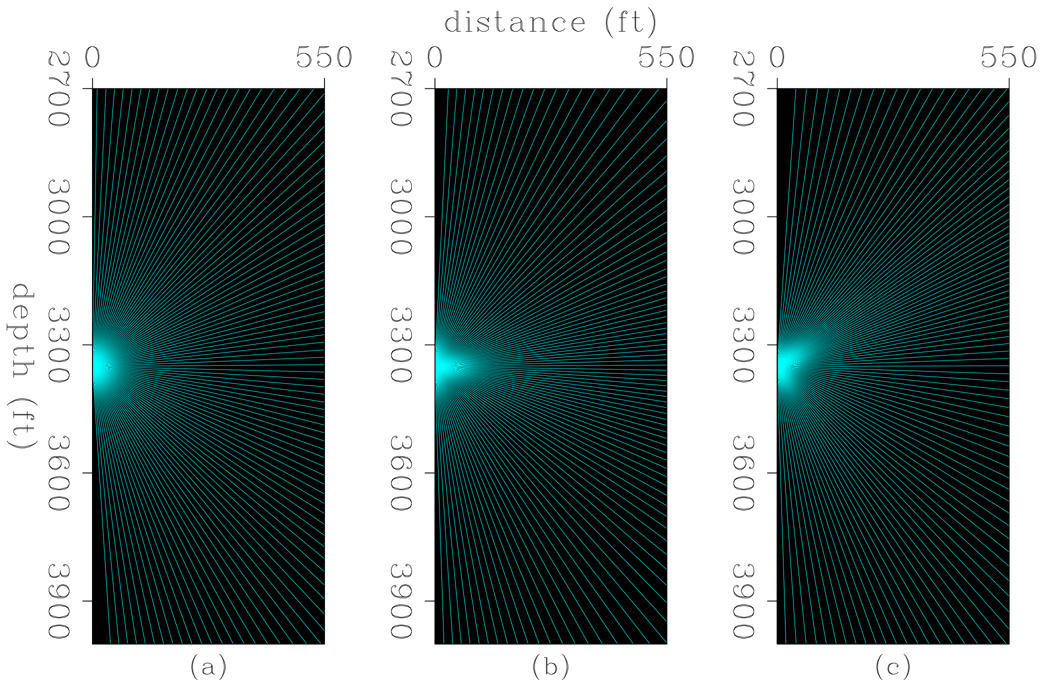

(a) (b) (c)

Figure 1.6: P-wave ray paths in different homogeneous models for a source located at 3350 feet. (a) Isotropic. (b) Transversely isotropic with vertical axis of symmetry. (c) Transversely isotropic with $\gamma = -30$. Note how the density of rays with angle changes in the anisotropic models. The elastic constants used in (b) and (c) are $(c_{11}/\rho)^{1/2} = 9894$, $(c_{33}/\rho)^{1/2} = 9005$, $(c_{44}/\rho)^{1/2} = 4949$, and $(c_{13}/\rho)^{1/2} = 5655$, all in (ft/s). The density ρ is assumed to be unity. rays-homo [NR]

Layer 1	Layer 2	Layer 3	Layer 4
$V_{11} = 9005$	$V_{11} = 9894$	$V_{11} = 12545$	$V_{11} = 9005$
$V_{33} = 9005$	$V_{33} = 9005$	$V_{33} = 10845$	$V_{33} = 9005$
$V_{44} = 4949$	$V_{44} = 4949$	$V_{44} = 5968$	$V_{44} = 4949$
$V_{13} = 5655$	$V_{13} = 5655$	$V_{13} = 6805$	$V_{13} = 5655$

Table 1.1: Elastic constants $V_{ij} = \sqrt{c_{ij}/\rho}$ [in (ft/s)] of the models shown in Figure 3.7. In all cases, the elastic constants are referred to the axis of symmetry of the corresponding layer. Layers are counted from top to bottom. The density ρ is assumed to be unity.

Figure missing !

Figure 1.7: Heterogeneous anisotropic models. Two of the four homogeneous blocks are anisotropic with the orientation of the axes of symmetry indicated by the arrows. The axis of symmetry is perpendicular to direction of fine layering. In both models, layers 1 and 4 (from top to bottom) are isotropic. The third block of thin layers in the model at the left ($\gamma = 0$) can be the result of deposition in an eroded boundary whereas the same block in the model at the right ($\gamma = 30$) can be the result of tilting after deposition over a plane boundary. The position of the source is shown by an asterisk ($*$). models [NR]

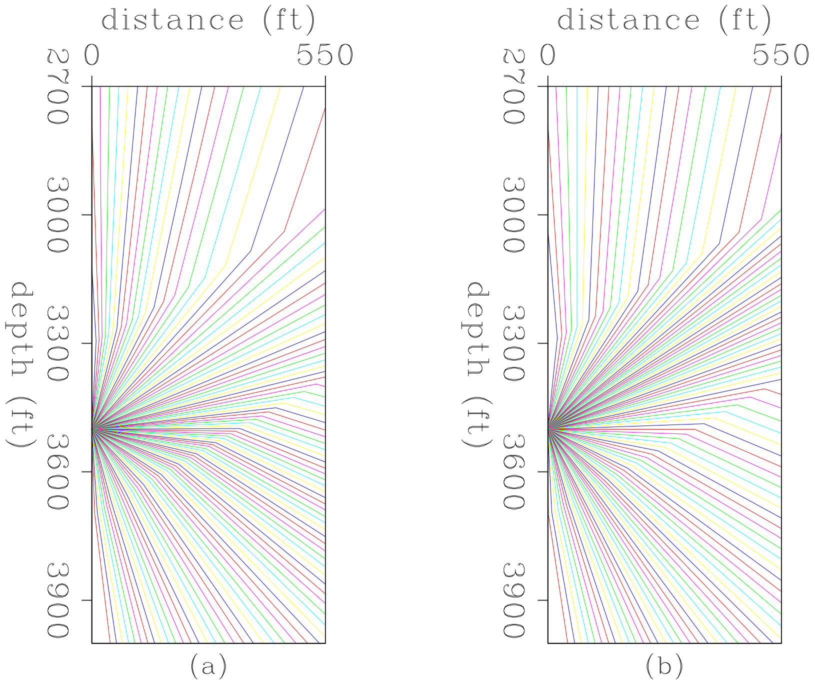

(a) (b)

Figure 1.8: P-wave ray paths in the models of Figure 3.7 for a source located at 3500 feet. (a) Vertical axis of symmetry. (b) Tilted axis of symmetry. rays-hete [NR]

1.8 Conclusions

This chapter has reviewed the basic steps for tracing rays in layered transversely isotropic models, emphasising the calculation of the angle of the transmitted phase as a function of the ray parameter of the incident phase. When the angle of incidence is small, I use a different procedure for estimating the angle of the transmitted phase than when the angle of incidence is large. In the latter case, the transmitted phase angles are calculated from the roots of a four-order polynomial in the tangent of the angle for P- and SV-waves and analytically for SH-waves. The appropriate root must reproduce the p of the incident

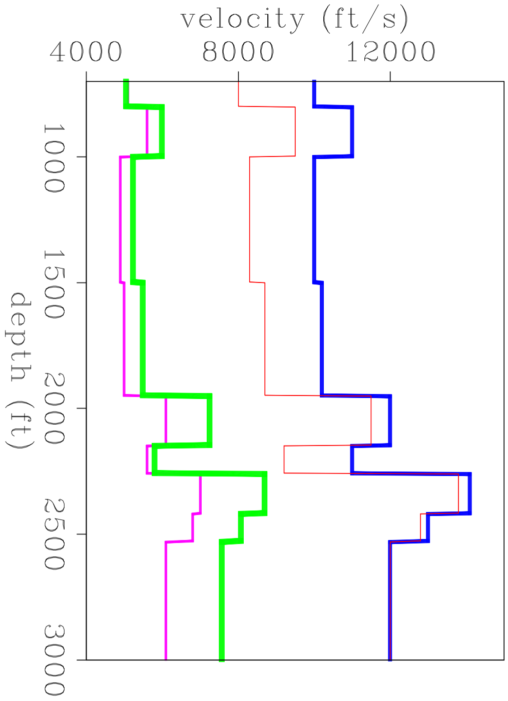

Figure 1.9: Elastic constants (in units of velocity) varying with depth. This model was used to run the ray tracing algorithm and compare the results with those of the finite-difference elastic modeling. From left to right the four curves represent $(c_{44}/\rho)^{1/2}$, $(c_{13}/\rho)^{1/2}$, $(c_{33}/\rho)^{1/2}$, and $(c_{11}/\rho)^{1/2}$, respectively. elastic-exact [NR]

phase for the given wave type, producing a ray in the desired direction.

The algorithm is tested by comparing the traveltimes calculated in a heterogeneous transversely isotropic model with those computed by finite-difference elastic modeling. Both sets of traveltimes are in perfect agreement.

In the next chapter, I use this method of anisotropic ray tracing as a part of a more general algorithm to do anisotropic traveltime tomography.

Figure missing !

Figure 1.10: Result of the finite-difference elastic modeling through the model shown in Figure 3.9. The dashed lines are created by ray tracing. Traveltimes of P-wave reflected arrivals from one interface have been also calculated by ray tracing. wave-vs-ray-reflect [NR]